Thermally Induced Reduction of the Load (TIRL) during Electron Beam Welding of CuCr1Zr

Ricardo Chin
ricardo.chin@tecnico.ulisboa.pt

Instituto Superior Técnico, Universidade de Lisboa, Lisboa, Portugal
October 2021

Abstract

Electron Beam Welding (EBW) is a highly efficient and precise welding method that is being increasingly used in industrial manufacturing and is of growing importance in industry. In the present study, solidification cracking in EBW of a CuCr1Zr cylindrical geometry was investigated. To analyze and avert occurrence of hot cracking, a thermomechanically coupled numerical model was built using Finite Element Method (FEM). An additional heat source was considered, in order to influence the resulting residual stress state, namely to minimize tensile stresses in the fusion zone during solidification. Hence, a systematic examination of relevant parameters, such as the power and the diameter of the additional heat source and the distances between both heat sources was employed using Design of Experiments (DoE) and a supervised learning algorithm Support Vector Machine (SVM). It was found that for a specific parameter configuration, solidification cracking most likely can be avoided.

Keywords: Electron Beam Welding, Numerical Simulation, Thermally induced reduction of the load, Design of Experiments, Support Vector Machine, Hot cracking;

1. Introduction

EBW is a fusion welding process where a narrow beam of electrons with high velocity is used to weld the two pieces of metals. The work pieces melt and partly evaporate as the kinetic energy of the electrons is transformed into heat upon interaction with the workpiece. The welding is usually carried out in vacuum to keep the energy density high [1]. Due to the high energy density, it can form a keyhole that results in deep and narrow welds. Thus, EBW remains indispensable in many aerospace, biomedical and mechanical applications namely due to a greater penetration depth, metallurgical purity of the weld, low heat input, small heat affect zone (HAZ) and low susceptibility to deformation. The development of numerical techniques like FEM has enabled researchers to overcome some practical difficulties such as complex boundary conditions, arbitrary geometry, and temperature dependent material properties [2]. Despite the technological innovations in FEM, there are still some problems when it comes to EBW, especially hot cracking. To solve this problem, other authors have tried to apply different experimental techniques, for instance, applying auxiliary heat sources on both sides of the weld to produce thermal gradients. However, such methodologies proved to be costly and time consuming [3], [4] creating the need for numerical studies which is exactly the goal of this work – a thorough numerical study on the hot cracking susceptibility in EBW of CuCr1Zr.

1.1 Material

Copper has outstanding electrical and heat transfer properties, moderately high-toughness and relatively high strength [5]. In this specific work, a copper alloy CuCr1Zr is used. This copper alloy contains small amount of chromium and zirconium which contribute to preserve excellent thermomechanical properties

E-mail address: ricardo.chin@tecnico.ulisboa.pt

of copper at high temperature and increase wear resistance. Due to the very low solubility of Cr and Zr in copper, the thermal conductivity is still high. The excellent strength is attributed to the precipitation and particle-dispersion strengthening mechanisms [6]. Chemical composition is represented in Table 1.

Fe	Si	Cr	Zr	Other	Cu
0-0,08	0-0,1	0,5-1,2	0,03-0,3	0,2	Bal.

Table 1 – CuCr1Zr chemical position in % [5]

1.2 Weldability of Cu-alloys

Welding defects can be defined as imperfections that compromise the usefulness of the welded parts. Defects in weld joints could result in the rejection of parts and assemblies, costly repairs, significant reduction of performance under working conditions and, in extreme cases, catastrophic failures with loss of property and life. Commonly seen defects in copper alloys are related with the presence of certain alloying elements that end up causing porosity due to their low boiling points or high percentage of oxygen in their chemical composition if enough quantities of deoxidizing elements are not present and hot cracking [7]. For EBW experiments performed on CuCr1Zr, a critical problem was the occurrence of hot cracks that were caused by high residual stresses.

1.3 Existent vs. Proposed Method

In EBW experiments of CuCr1Zr, hot cracking can be critical. A proposed solution for minimizing tensile residual stresses during solidification was explored. One possible solution to minimizing welding residual stresses actively is using the Low Stress No Distortion technique (LSND) which employs auxiliary cooling or heating sources to manipulate thermal gradients, generating a specific temperature field altering the stresses occurring in the weld zone. A comparison between the magnitude on the residual stresses can be seen in Figure 1, using LSND and conventional welding [4].

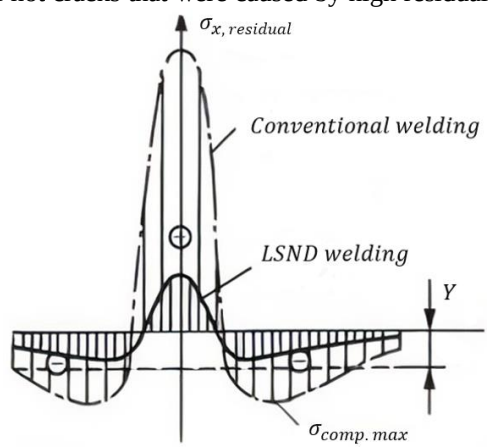

Figure 1 - Residual Stresses comparison using LSND vs. conventional welding [4]

These treatment processes are often either time-consuming, can end up increasing the cost and may also change the micro structures and mechanical properties [8]. A different alternative proposes a main welding beam while simultaneous multi-beam preheating on the side of the weld [9], [10]. Zhang *et al.* [9] found that the main advantages of this process over others, is that other processes need to employ complicated, heavy and costly additional facilities to generate heating or cooling source, while this method uses electromagnetic deflection to generate both welding and pre-heating beams, so there is no need to use auxiliary heating or cooling devices. Another advantage is the fact that due to EBW's characteristics; pre-heating beams can be generated as small as needed, making it possible to produce localized pre-heating areas with any geometric shapes and sizes. Based on these approaches a procedure is presented and investigated in this work. In this procedure, a Thermally Induced Reduction of the Load (TIRL) is applied where an additional Secondary Heat Source (SHS) introduces compressive stresses during the solidification of the weld pool through a local treatment while the Main Heat Source (MHS) associated with the welding process causes melting. The essential parameters of the SHS: the angle, radial distance, power and the representative dimension of the SHS are summarized in Figure 2.

Angle between MHS and SHS (°)	Radial distance between MHS and SHS (mm)	Power of SHS	Representative dimension of SHS: D_{SHS} (mm)
α	**d**	**P**	**D**
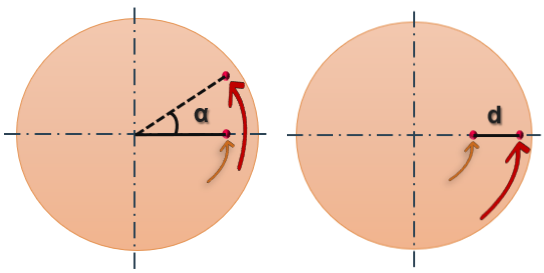		P_{MHS}* = 2.8 kW P_{SHS} = % of P_{MHS}	D = 0.075mm**
		* P_{MHS} is the power of the main heat source	**This is an arbitrary initial value

Figure 2 – SHS parameters

One factor at a time (OFAT) approach was applied to establish the value ranges for the aforementioned parameters. Subsequently, a systematic experimental approach using DoE was employed to assess statistical significance of the parameters and yield an optimum solution that avoids solidification cracking. A schematic representation of the methodology applied is presented in Figure 3.

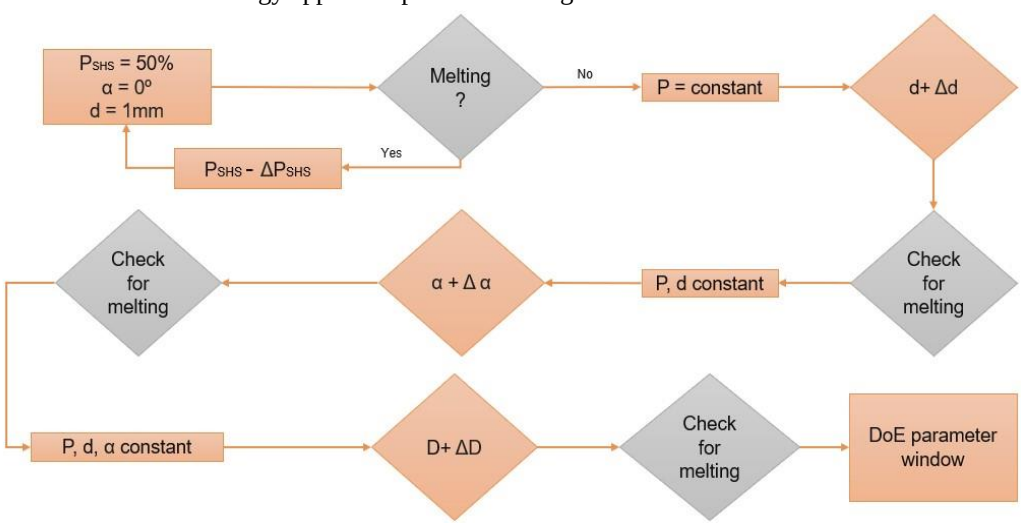

Figure 3 - Flowchart depicting the methodology implemented to define the working range of process parameters

The condition whether melting was occurring due to the SHS was verified at all steps. For instance, after having a parameter window for the power applied, it was possible to adjust the radial distance until no melting occurred whilst ensuring maximum introduced compressive stresses. This was performed successively until a parameter window was defined for all parameters.

2. Numerical Implementation

The software Simufact Welding was used for the FEM simulations. Simufact Welding is designed for modeling and simulation of a wide range of thermal joining processes. Additionally, it provides possibilities to model heat treatment processes, variations of cooling and unclamping setups as well as mechanical loading of welded structures making it suitable for these types of thermal and thermomechanical simulations. Numerical implementation methodology applied for this framework was widely based on [11]–[13]. At Firstly, a cylinder geometry was modeled using SolidWorks as can be seen in Figure 4.

Figure 4 – Geometry assembly

2.1 Geometry Discretization

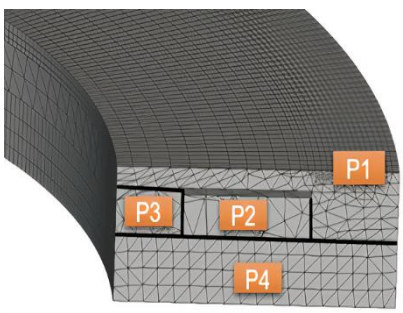

Figure 5 – Geometry discretization

The detailed geometry is omitted from this thesis due to confidentiality reasons. In terms of discretization of the domain, the simplified model built was an assembly of 4 components as is shown in Figure 5 which included a total of 97794 elements. In the case of P1 and P4 hexahedral elements were chosen for its improved quality over tetrahedral elements. Tetrahedral elements were chosen for P2 and P3 due to their simple shapes, therefore easing computation for arbitrarily complex volume and surface integrals in FEM, given that the quality for these parts was not considered as important [14]. The mesh was refined where the heat source's path (P1) was located. The other components (P2, P3 and P4) had a coarse mesh.

2.2 Material Mechanical and Thermophysical Properties

Since the material properties of CuCr1Zr alloy were not available in Simufact material library, a similar alternative was used. Material's thermophysical and mechanical properties are described in Table 3.

1) Thermophysical Properties (20°C)	**Unit**	**CuCr1Zr** [5]	**Cu_SW**
Density	g/cm^3	8.89	8.86
Melting Temperature	°C	1076	1084
Thermal Conductivity	W/(m.K)	170	182
Specific Heat Capacity	J/(kg K)	380	414
2) Mechanical Properties (20°C)			
Tensile Stress	MPa	380	380
Yield Stress	MPa	300	300
Hardness Brinell	HB	130	N/A
Young Modulus	GPa	128	129

Table 3 – Material properties

2.3 Heat Source Model

The software uses the heat source models developed by Goldak *et al.* [15]. For heat distribution description in deep and narrow welds such as the ones produced by means of electron beam or laser beam, a conical heat source model seems to be more suitable. Heat source characteristics can be seen in Equations **(1)** and **(2)**.

$$Q(x,y,z) = \frac{\eta P}{v} e^{-M\frac{x^2+y^2}{r_0^2(x)}} \quad \textbf{(1)}$$

$$where\ r_0 = r_e + \frac{r_i - r_e}{z_i - z_e}(z - z_e) \quad \textbf{(2)}$$

The heat source model parameters: conical upper radius (r_e), conical lower radius (r_i), gaussian parameter (M), conical depth ($d_c = z_i - z_e$) were regulated using sensitivity analysis. Thermal simulations were conducted to calibrate process efficiency based on the experimental weld dimensions provided by the company. A short trajectory was chosen, the geometry used for the experiment was a flat plate with 15mm of thickness, 400mm length and 150mm width and the process parameters considered for the experiment were 120 kV voltage, 12.5 mA beam current and a welding velocity of 20mm/sec. An efficiency of 93.5% was attained and the corresponding weld dimensions numerical (case a.) vs. experimental (case b.) are shown in Figure 6.

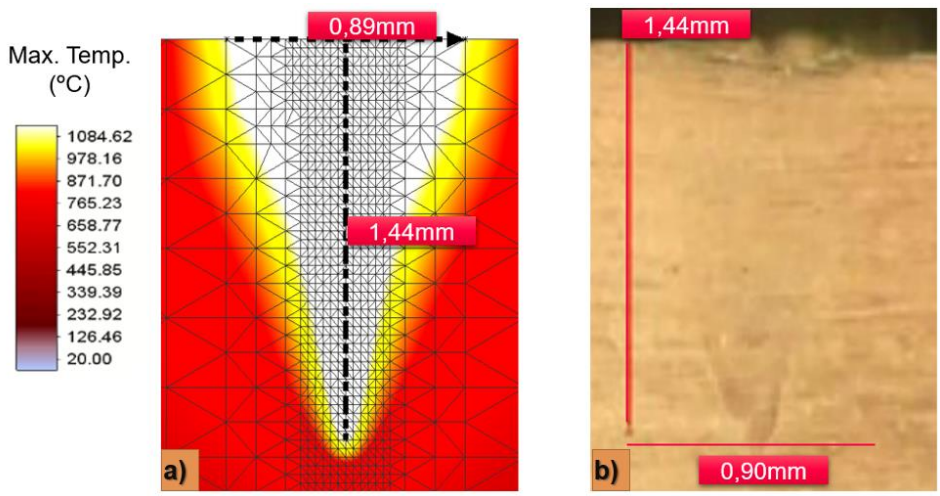

Figure 6 – Cross-section highlighting the fusion zone: a) Numerical and b) Experimental result

A conical heat source was used with an upper diameter and lower diameter of 0,15 and 0,125, respectively, and a conical heat source depth of 1,565. Gaussian parameter was set to 3. The minor difference between numerical and experimental weld dimensions could be addressed due to slight approximations that were considered when performing sensitivity analysis for the heat source model. Furthermore, the efficiency calibration was fully dependent on the aforementioned analysis.

3. Results and Discussion

Having successfully performed an assessment on the MHS such that all influential heat source model parameters were known, it was possible to evaluate the stress distribution conducting thermomechanical simulations. The results for these simulations were exported to an Excel file and compared to the temperature dependent strength of the material. The condition for no hot cracking is given by:

$$\sigma_{stress} < \sigma_{proof}$$

This criterion states that if the stresses were smaller than the admitted proof stress of the material, then hot cracking would not occur. The statistical software Minitab 19 was used to obtain an optimal solution for the SHS parameter configuration minimizing the stress to proof stress ratio.

3.1 No secondary heat source

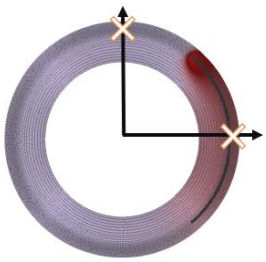

A thermomechanical simulation without the use of a secondary beam was employed and provided an overview on the residual stresses. This evaluation was performed on points selected aligned with the X-axis and Y-axis (as is shown in Figure 7) given that the X-stress and Y-stresses at these points, respectively, are entirely equal to the radial stresses (that cause hot cracking). Furthermore, multiple points equally spaced in depth were considered to verify if cracking would, in fact, firstly emerge on the surface of the material.

Figure 7 – Point selection

It was not necessary to check the stress values for the other points below the surface since cracking always occurred over the surface. To further understand the ratio and to ease the evaluation on occurrence of hot cracking, the ratio was plotted over time as can be seen in Figure 8. Hence, it can be acknowledged that cracking had occurred since the relation yielded a value greater than 1.

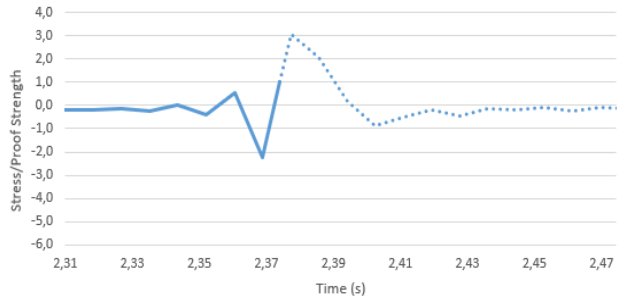

Figure 8 – Ratio between stress and proof stress over time on the surface of a pre-selected point in the weld line. Dashed line represents case of hot cracking

3.2 OFAT

Arbitrary values were assumed for an initial condition (d = 1mm, P = 50% and $\alpha = 0^{o}$, D was set to the same value as considered for the MHS to simplify first simulations). It was concluded that utilizing a SHS with those characteristics too close to the MHS would produce a merge in the fusion zone, melting even more material than intended. To avoid melting by the SHS a sensitivity analysis using the OFAT approach was selected on the Power, keeping all other variables constant. By iteratively lowering the power, it was seen that for this angle and radial distance ($\alpha = 0^{o}$ and d = 1mm), 2.5% was the maximum power that could be employed without secondary melting. Subsequently, an assessment keeping the power constant and $\alpha = 0^{o}$ while adjusting the radial distance was executed followed by a study on the angle. However, it was concluded that the variation of the angles was very small ($\approx 0°$), so hereafter this variable is described as the tangential distance **(**dt**)** allowing for easier understanding. Multiple tests were conducted for the surface diameter of the SHS, ranging from as low as D = 0.075mm up to as high as D = 5mm, but the results did not vary that much.

3.3 Design of Experiment (DoE)

Having gathered understanding of the impact of each variable on the outcome of the simulations, the next step would be to build a parameter window for the DoE. A full factorial design (FFD) was chosen due to its reliability and capacity of giving information on how each factor is correlated with each other [16], [17]. A 3-level full factorial DoE with 4 factors was initially chosen, Table 4. Thus, 81 simulations were conducted.

Factor	Levels	Level 1	Level 2	Level 3
d [mm]	3	2	3	4
P [%]	3	35	40	45
dt [mm]	3	-3	-1	1
D [mm]	3	2	3	4

Table 4 – 3-level full factorial DoE with 4 factors

To improve this first attempt, Analysis of Variance (ANOVA) was conducted from which resulted the identification and elimination of irrelevant factors and levels [18]–[20]. Hence, D was dropped and a modified DoE with 3 factors at 2 levels was carried out, as can be seen in Table 5. The tangential distance levels were considered as dt = 3.5mm and dt = 3mm and the radial distance levels between both were d = 2mm and d = 2.5mm. The power levels were increased to 45% and 50% since increasing the power reproduced better results.

Factor	Levels	Level 1	Level 2
d [mm]	2	2,0	2,5
P [%]	2	45	50
dt [mm]	2	-3,5	-3,0

Table 5 – 2-level full factorial DoE with 3 factors

The modified final DoE was further improved from the analysis of the Pareto charts of standardized effects for a significance level of 5%. Therefore, all the unnecessary factors and interactions were also removed (interaction between tangential distance and both radial distance and power – AC and BC – as is presented in Figure 11), and the model obtained had predicted R^2 of 99,55%. The statistical results are presented in Table 6.

S	R^2	R^2 (adjusted)	R^2 (predicted)
0,01	99,97%	99,90%	99,55%

Table 6 – Modified DoE statistical results

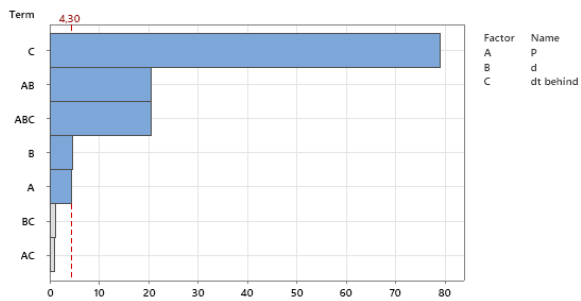

Figure 9 – Pareto chart for the standardized response of the modified DoE for 5% significance level

The relations between the response and two other factors were extracted and evaluated through contour charts using the software Minitab 19 [19] and are displayed in 13.

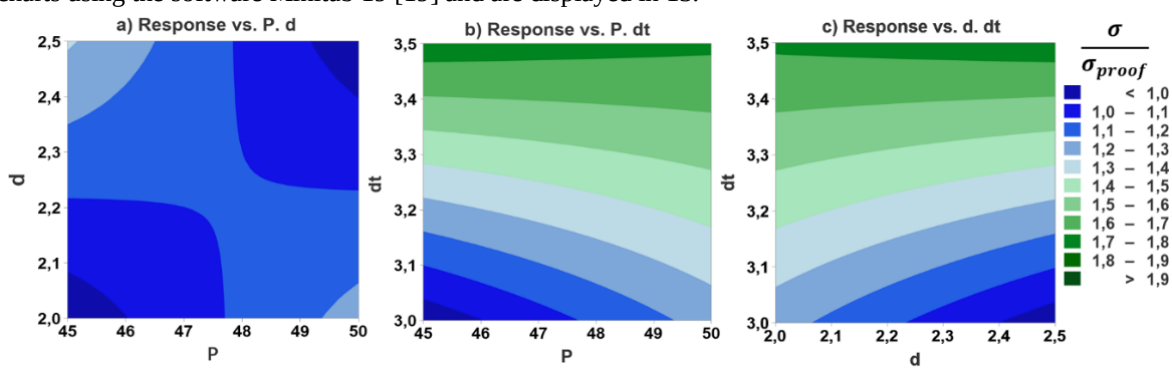

Figure 10 – **a)** Response vs. P. dt – **Held value** dt = 3mm; **b)** Response vs. P. dt – **Held value** d = 2mm ; **c)** Response vs. d. dt – **Held value P** = 50%

An interesting result can be obtained from Figure 14a) which displays the connection between the radial distance of both heat sources and the power applied while retaining the tangential distance constant at

3mm. The results improved with a relative parabolic increase of power and radial distance – increasing power needed a higher distance between both heat sources; whereas a lower power would allow a reduced distance between both heat sources to replicate similar reasonable results. This makes sense given that when the temperature is near the melting temperature, the results are worsened. Case b) relates the tangential distance between heat sources and the Power. Conducting experiments with a combination of smaller tangential distances and power applied proven to be beneficial. It can also be concluded that the power seemed to barely change the outcome, given that the tangential distance had a way bigger impact. Lastly, case c) presents the effect on the response, considering the radial and tangential distance of both heat sources. The results for this case were extracted keeping the power at a constant value of 50%. Similarly, to the case b), the radial distance displayed greater impact for lower values of the tangential distance. The response is given by the following regression equation **(3)**.

$$\mathbf{Y(P, d, dt)} = 1{,}43158 - 0{,}01807\,\mathrm{P} + 0{,}01907\,\mathrm{d} + 0{,}32493\,\mathrm{dt} - 0{,}08458\,\mathrm{P}\cdot\mathrm{d} + 0{,}08407\,\mathrm{P}\cdot\mathrm{d}\cdot\mathrm{dt} \quad \textbf{(3)}$$

The response optimizer in Minitab allows to identify the combination of input variables that optimize a single response. It calculates an individual desirability for each response and weights each by the importance. [19], [21]. In this case, equation **(3)** was to be minimized. The results showed significant improvement when compared to the first trials, there were multiple feasible solutions from which hot cracking could be mitigated as seen in Table 7. Promising parameter combinations were from 1 to 5.

Combination	P (%)	d (mm)	dt (mm)	Y(P,d,dt)
1	45,00	2,00	-3,00	0,9370
2	50,00	2,50	-3,00	0,9390
3	49,99	2,49	-3,00	0,9415
4	45,21	2,00	-3,01	0,9522
5	50,00	2,47	-3,00	0,9529
6	45,98	2,40	-3,00	1,1907
7	45,07	2,49	-3,00	1,3012
8	50,00	2,00	-3,50	1,7199

Table 7 – Solutions for the minimization of the ratio between stress and proof stress based on the DoE model

Numerical validation was carried to assess the adequacy of the statistical model, thus condition 1 was selected for a final experiment as can be seen in Figure 11. The peak temperature of the SHS at different times throughout the simulation was 1020ºC. Weld dimensions were respected. As it is seen in Figure 12, hot cracking did not seem to occur (stress/proof stress<1) under these conditions, so a solution was found and thus, confirming that the TIRL method is suitable to avoid hot cracking in CuCr1Zr.

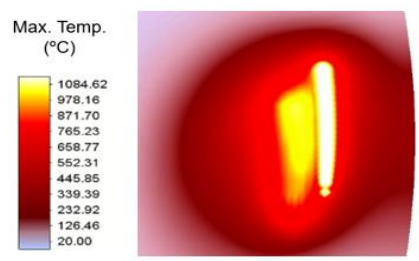

Figure 11 – Peak temperature at different times

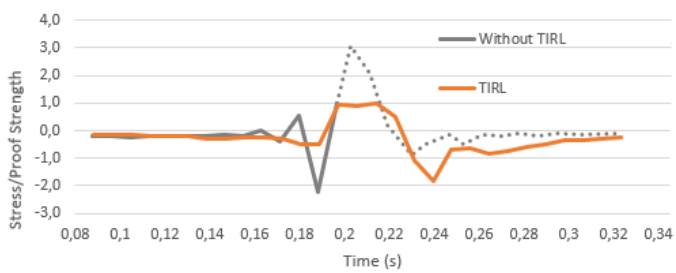

Figure 12 – Stress evaluation over time on the surface with and without TIRL. Dashed line represents case of hot cracking

3.4 Support Vector Machine (SVM)

A different approach was conducted using the Support Vector Machine (SVM) algorithm. The key point is that it doesn't rely on a larger training data sample as the DoE. A total of 67 data samples were used for this model. From previous results using other methodologies, results were non-linear, so a polynomial kernel was selected for the boundary condition of this SVM model. The data was split into two different sets: a training set and a testing set, 67% and 33%, respectively. Despite the good fit for the data (approx.. 95% acc.), the model build was not good enough as can be seen in Figure 13.

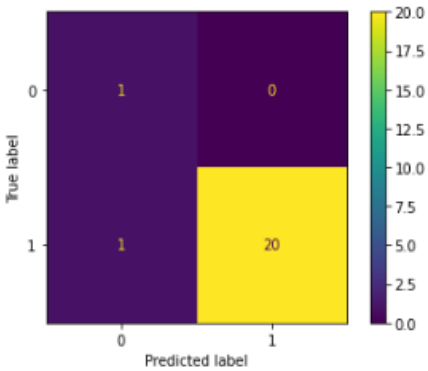

Figure 13 – Confusion matrix

It was concluded that in one of the cases, the model predicted that there was no cracking occurring when, in reality, that was not the case. The unbalanced classification and the limited available data (especially for the no-cracking region where points of interest are located) create the need for generalization through cross-validation which is a powerful tool that measures the model's efficiency scores for selecting the best model for a given task. In this specific case, the leave-one-out cross-validation 67-fold was used to assess the model's practicability. To evaluate the model built, results such as: accuracy, precision and recall were extracted from each conducted experiment. A single measure to compare between models was taken from the average scoring across all experiments as is seen in Table 8.

Leave-one-out cross-validation scoring results	
Accuracy (%)	98.48
Mean Square Error (%)	1.52
Precision (%)	92.42
Recall (%)	92.42

Table 8 – Leave-one-out cross-validation scoring results

Across all experiments, the precision or positive predictive value was, on average, equal (92.42%) to the recall or true positive rate which considers the ratio of correct positive predictions over the total positive examples. This was an attempt to improve computing efficiency. Moreover and unlike DoE, SVM models are much less prone to overfitting (in the case of DoE, the model was heavily tuned to provide the best results) as it is also one of the its advantages: to "think outside the box" when using relatively small training data samples.

4. Summary and Conclusion

The main conclusions arising from the work done in the framework of this thesis are presented and categorized according to the issues addressed. Results enhanced with the OFAT, DoE and SVM methods, but it is uncertain that this solution is a global optimal.

- The influence of each parameter individually and amongst each other was assessed based on the stress magnitude alteration. The tangential distance (or angle) had the greatest impact on introducing compressive stresses during solidification while the diameter of the SHS had the least impact;
- Smaller distances between heat sources or higher power for the SHS could cause secondary fusion of the material (and possible merge of the fusion zones);
- Longer distances between heat sources were proven to be meaningless, given that solidification for this specific alloy occurred very fast;

- The work performed confirms that numerically it is possible to reproduce electron beam welds in CuCr1Zr whilst avoiding the occurrence of hot cracking utilizing the TIRL method.

References

[1] G. Schubert, "Electron beam welding- Process, applications and equipment," 2009.

[2] G. R. Liu and S. S. Quek, *Finite Element Method: A Practical Course*. Elsevier Ltd, 2003.

[3] H. Wibowo, M. N. Ilman, P. T. Iswanto, and M. R. Muslih, "Reducing Distortion and Residual Stress Using Dynamically Controlled Low Stress No Distortion and Its Influence on Fatigue Crack Growth Properties of Steel Welded Joints," *Trans. Indian Inst. Met.*, 2019, doi: 10.1007/s12666-018-1469-7.

[4] Q. Guan, "Low stress no distortion welding based on thermal tensioning effects," *Avtom. svarka*, 2018, doi: 10.15407/as2018.12.05.

[5] J. Freudenberger and H. Warlimont, "Copper and copper alloys," in *Springer Handbooks*, 2018.

[6] "The Welding Institute," in *Quality Technology Handbook*, 1984.

[7] "Weldability of Materials - Copper and Copper Alloys - TWI." https://www.twi-global.com/technical-knowledge/job-knowledge/weldability-of-materials-copper-and-copper-alloys-023

[8] S. WANG, Y. HUANG, and L. ZHAO, "Effects of different aging treatments on microstructures and mechanical properties of Al-Cu-Li alloy joints welded by electron beam welding," *Chinese J. Aeronaut.*, 2018, doi: 10.1016/j.cja.2017.07.002.

[9] W. Zhang *et al.*, "Influence of multi-beam preheating temperature and stress on the buckling distortion in electron beam welding," *Mater. Des.*, 2018, doi: 10.1016/j.matdes.2017.11.016.

[10] J. Fan, W. Zhang, B. Qi, and F. Liu, "Influence of Multi-Beam Electron Beam Welding Technique on the Deformation of Ti6Al4V Alloy Sheet," *Xiyou Jinshu Cailiao Yu Gongcheng/Rare Met. Mater. Eng.*, vol. 46, no. 9, pp. 2417–2422, Sep. 2017, doi: 10.1016/s1875-5372(17)30208-4.

[11] M. Chiumenti, M. Cervera, N. Dialami, B. Wu, L. Jinwei, and C. Agelet de Saracibar, "Numerical modeling of the electron beam welding and its experimental validation," *Finite Elem. Anal. Des.*, vol. 121, pp. 118–133, Nov. 2016, doi: 10.1016/j.finel.2016.07.003.

[12] P. Lacki and K. Adamus, "Numerical simulation of the electron beam welding process," in *Computers and Structures*, Jun. 2011, vol. 89, no. 11–12, pp. 977–985, doi: 10.1016/j.compstruc.2011.01.016.

[13] R. SINGH, S. SINGH, P. K. C. KANIGALPULA, and J. S. SAINI, "Electron beam welding of precipitation hardened CuCrZr alloy: Modeling and experimentation," *Trans. Nonferrous Met. Soc. China (English Ed.*, vol. 30, no. 8, pp. 2156–2169, Aug. 2020, doi: 10.1016/S1003-6326(20)65368-7.

[14] J. N. Reddy, "An Introduction to The Finite Element Method (third Edition)," *McGraw-Hill*, 2005.

[15] J. A. Goldak and M. Akhlaghi, *Computational welding mechanics*. 2005.

[16] J. Antony, *Design of Experiments for Engineers and Scientists*. Elsevier Ltd, 2003.

[17] J. Antoy, *Design of Experiments for Engineers and Scientists: Second Edition*. Elsevier Ltd, 2014.

[18] A. Raj, J. Pratap Kumar, A. Melwin Rego, and I. Sunit Rout, "Optimization of friction stir welding parameters during joining of AA3103 and AA7075 aluminium alloys using Taguchi method," *Mater. Today Proc.*, Mar. 2021, doi: 10.1016/j.matpr.2021.02.246.

[19] "Minitab," *Comput. Stat. Data Anal.*, vol. 1, pp. 55–57, Mar. 1983, doi: 10.1016/0167-9473(83)90065-8.

[20] M. Arab and M. Zemri, "Optimization of process parameters on friction stir welding of AA 6082-T6 butt joints using Taguchi method," *Mech. Mech. Eng.*, vol. 22, no. 4, pp. 1371–1380, 2018, doi: 10.2478/mme-2018-0107.

[21] H. Singh, V. Kumar, and J. Kapoor, "Multi-response optimization of WEDM process parameters during the fabrication of microchannels for industrial applications," *Mater. Today Proc.*, Jul. 2020, doi: 10.1016/j.matpr.2020.06.134.